# A NOVEL CONCEPT ON THE PLASMA GURNEY FLAP

**Li-Hao Feng\*, Jin-Jun Wang\*, Kwing-So Choi\*\***
**\*\*Faculty of Engineering, University of Nottingham, Nottingham NG7 2RD, UK**
**\*Fluid Mechanics Key Laboratory of Education Ministry, Beijing University of**
**Aeronautics and Astronautics, Beijing 100191, P. R. China**
*lhfeng@buaa.edu.cn*

**Keywords**: *Flow control, Plasma Gurney flap, Airfoil*

## Abstract

*An experiment is conducted to simulate the lift increment function of the mechanical Gurney flaps by the dielectric barrier discharge (DBD) plasma actuators, which is named as the plasma Gurney flap. Three different kinds of the plasma Gurney flap have been proposed. For configurations 1 and 2, two DBD plasma actuators are placed onto the pressure (lower) surface of the airfoil near the trailing edge to produce a wall-normal jet, with a distance from the downstream edge of the second electrode to the airfoil trailing edge 1 mm and zero, respectively. For configuration 3, only one DBD plasma actuator is positioned onto the airfoil pressure surface to produce a horizontal wall jet opposite to the free stream. The force measurement indicates that the configuration 3 can most significantly improve the lift coefficient, while configuration 1 has little influence on the aerodynamic forces. The PIV measurement indicates that the flow topology around the airfoil induced by the configuration 3 is similar to that induced by the mechanical Gurney flap, suggesting a similarity in their lift-increment mechanism.*

## 1 Introduction

The Gurney flap can enhance the aerodynamics performance of low-speed, subsonic and supercritical airfoils, high-lift devices, delta wings and aircrafts [1]. It is easy to implement the Gurney flap since it is a simple flat plate attached on the pressure side of the airfoil. Many researchers have used the Gurney flap to control the flow around an airfoil [2-5]. It was found that the Gurney flap could increase the lift coefficient and the increment increased with the Gurney flap height. The lift increment is because of the increase in both the suction surface pressure and the lower surface pressure. However, accompanied with the lift increment, there is also an inevitable drag penalty. Therefore, the active control ability of the Gurney flap is of great significance.

A good alternative is the jet Gurney flap. Traub et al. [6] conducted an experimental investigation on the control of a NACA 0015 airfoil with the continuous jet. The jet-issuing slot was located at 2% chord upstream of the trailing edge. It was found that jet control with momentum coefficient of 0.68% could result in lift and momentum increases equivalent to a 0.75% chord mechanical Gurney flap. Traub and Agarwal [7] further undertook an investigation to establish the effect of the Gurney flap in conjunction with the jet flap at low Reynolds numbers. The jet forcing could further increase the lift coefficient of the airfoil installed with the mechanical Gurney flap. The control effect maintained a theoretically determined dependence on the jet momentum coefficient.

Similar with the continuous jet generated by an air pump, the dielectric barrier discharge (DBD) plasma actuator can also induce a wall jet [8]. The DBD plasma actuator usually consists of an exposed electrode and an embedded electrode, separated by a dielectric sheet. The electrodes are supplied with high voltage and frequency, causing the air over the embedded electrode to ionize and thus form a

wall jet. More details about the DBD plasma actuator can be found in the review papers [9-11].

Zhang et al. [12] numerically investigated the effect of a plasma Gurney flap on the aerodynamic characteristics of a NACA 0012 airfoil. The plasma actuator was assumed to adhere to the cut section of the trailing edge. The results indicated that the plasma Gurney flap could increase the lift and nose-down moment of the airfoil in the same way as the conventional Gurney flap. It was also shown that the Kármán vortices disappeared near the trailing edge of the airfoil, which reduced the airfoil's drag and thus enhanced the lift-to-drag ratio before stall.

In this study, an experiment is conducted to simulate the lift-increment function of the mechanical Gurney flaps by the DBD plasma actuators, which is named as the plasma Gurney flap. Several different kinds of the plasma Gurney flap have been proposed. The control effects have been compared and the optical one has been concluded. The control mechanism is also revealed based on the flow field measurement by particle image velocimetry (PIV).

## 2  Experimental Set-up

The experiment was conducted in a low-speed open-return wind tunnel with a 1.5 m × 0.3 m × 0.3 m test section. The experimental model was a NACA 0012 airfoil with chord length $c$ = 100 mm and span $b$ = 250 mm. The free-stream velocity was set at $U_\infty$ = 3.0 m/s, corresponding to the Reynolds number $Re$ = 20,000 based on the airfoil chord length. End-plates of 300 mm × 200 mm in the streamwise and vertical directions were mounted 25 mm from the wind tunnel walls to maintain the two-dimensionality of the flow field. Here, the coordinate origin was fixed at the trailing edge of the airfoil at 0° angle of attack, with the $x$ and $y$ axes pointing to the streamwise and vertical directions, respectively.

The DBD plasma actuators were placed on the airfoil pressure (lower) surface. Figure 1 shows the basic configuration, which consists of two asymmetric DBD plasma actuators attached to the pressure surface of the NACA 0012 airfoil near the trailing edge. Based on the basic characteristics of the DBD plasma actuators, each actuator powered at high voltage and high frequency will produce a wall jet moving against to each other in the center of the DBD plasma actuators and roll up to form a normal jet. It is proposed that the normal wall jet induced by the DBD plasma actuators can simulate the flow blocking effect of the mechanical Gurney flaps.
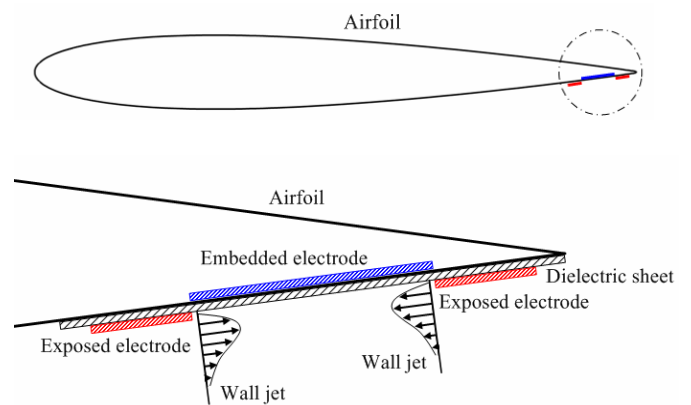


Fig. 1 DBD plasma actuators attached to the airfoil.

For the force measurement, three different kinds of the DBD configurations were tested for comparison. For the first two configurations, the width of each exposed electrode and the embedded electrode was 1 mm and 4 mm, respectively. The DBD plasma actuators were supplied at high AC voltage of 6 kVp-p and high frequency of 18 kHz. The only differences between these configurations were that the distance of the downstream edge of the right exposed electrode to the airfoil trailing edge was 1 mm and zero, respectively, which we call configuration 1 and configuration 2. On the other hand, configuration 3 consisted only of a downstream plasma actuator (see Fig. 1). Thus, there would be a horizontal wall jet induced by the plasma actuator with its direction opposite to the free stream. For the flow field measurement, only configurations 1 and 3 were compared, where the width of exposed electrode and the embedded electrode was 2.5 mm and 6 mm, respectively. The distance of the downstream

edge of the second electrode to the airfoil trailing edge was 1 mm for both configurations. Configuration 1 was powered sinusoidally at an AC voltage of 8 kVp-p with frequency of 19 kHz, while configuration 3 was powered at an AC voltage of 10 kVp-p with frequency of 18 kHz.

The lift and drag coefficients were measured by a two-component dynamic force balance. More details about the force balance can be found in Jukes and Choi [13]. The airfoil model was mounted on the force balance through a rod located at the middle axis of 25%$c$ from the leading edge. The calibration result showed that the absolute accuracy of the force measurement was better than ±0.01 N. The uncertainty of the airfoil attack angle during experiments could be kept within ±0.25˚.

The flow field was measured by the time-resolved PIV system. The field of view was illuminated by a light sheet using a Nd:YLF laser system. The seeding particles were approximately 1 μm diameter droplets generated from olive oil. The digital image sets were captured by a Phantom V12.1 high-speed camera with a spatial resolution of 1280 pixels × 800 pixels in the streamwise and vertical directions, respectively. The sampling frequency was 2 kHz. For each test case, 4000 image pairs were recorded continuously, with the first 2000 image pairs without plasma control and the rest with plasma control. The Dantec Dynamic Studio v3.00 was used to calculate the velocity field. The interrogation window was set to 32 × 32 pixels with 50% overlap in both streamwise and vertical directions. A relative correlation algorithm was used to compute the velocity vector maps.

## 3 Results and Discussion

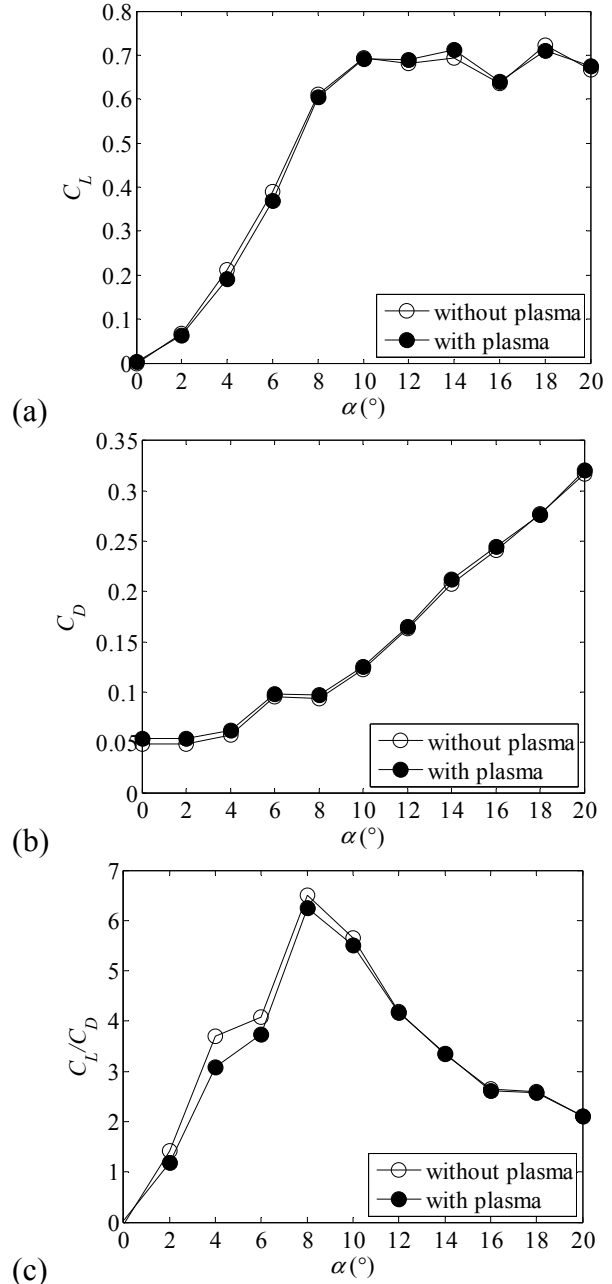### 3.1 Aerodynamic Forces



(a)

(b)

(c)

Fig. 2 Lift coefficient of the airfoil without and with plasma control of configuration 1, where two DBD plasma actuators are used. The width of each exposed electrode and the embedded electrode is 1 mm and 4 mm, respectively, and the distance of the downstream edge of the right exposed electrode to the airfoil trailing edge is 1 mm. (a) Lift coefficient; (b) drag coefficient; (c) lift-to-drag ratio.

Figure 2 shows the aerodynamic forces for the airfoil without and with plasma control for configuration 1. It is found that the plasma control has little influence on both the lift and drag coefficients. There is even a small decrease

in lift coefficient before stall and an increase in drag during the whole angles of attack. As a result, the lift-to-drag ratio is slightly reduced by plasma control. Thus, configuration 1 of plasma Gurney flap does not achieve the objective of lift improvement.
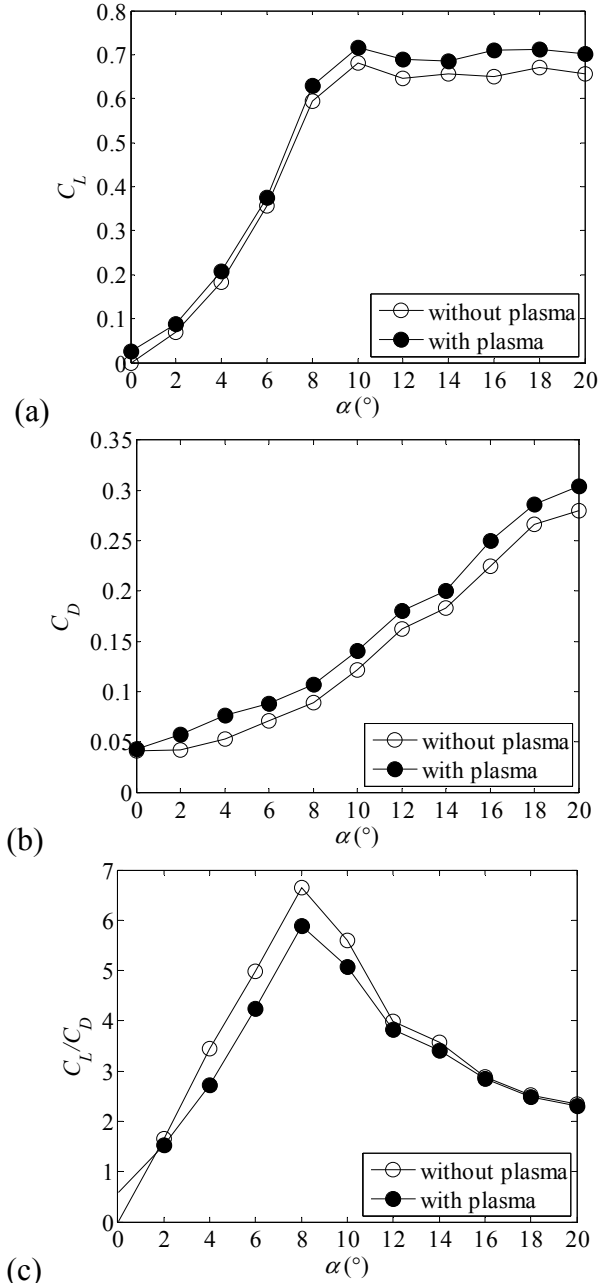


(a)



(b)



(c)

Fig. 3 Lift coefficient of the airfoil without and with plasma control of configuration 2, where two DBD plasma actuators are used. The width of each exposed electrode and the embedded electrode is 1 mm and 4 mm, respectively, and the distance of the downstream edge of the right exposed electrode to the airfoil trailing edge is zero. (a) Lift coefficient; (b) drag coefficient; (c) lift-to-drag ratio.
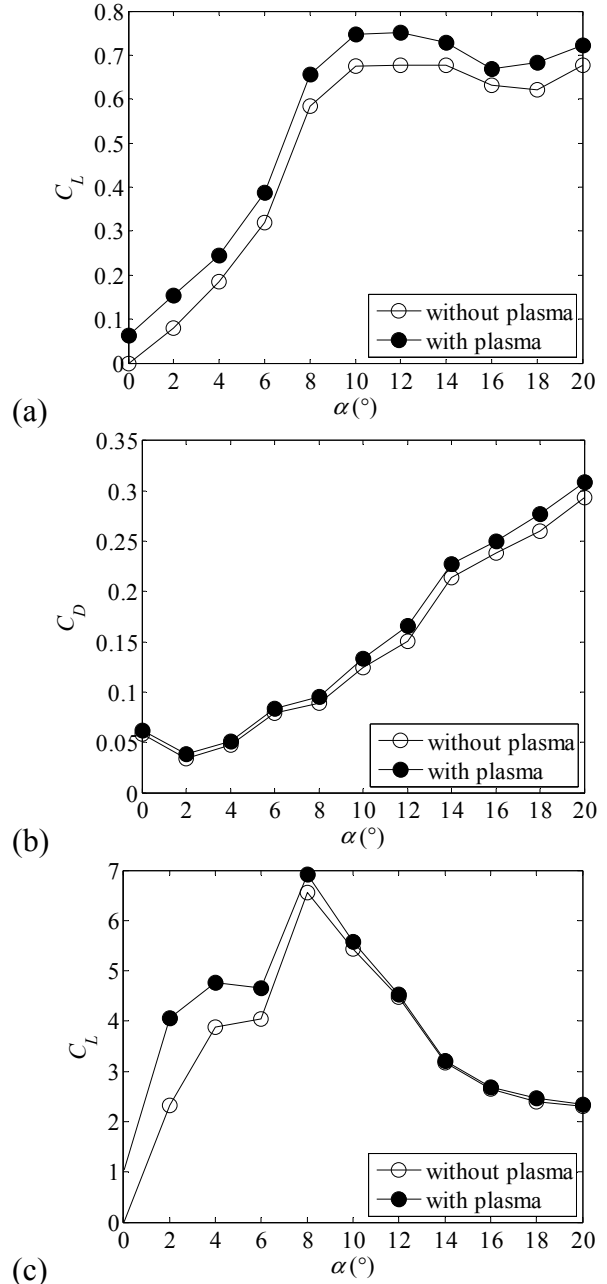


(a)



(b)



(c)

Fig. 4 Lift coefficient of the airfoil without and with plasma control of configuration 3, where one DBD plasma actuator is used. The width of the exposed electrode and the embedded electrode is 1 mm and 4 mm, respectively, and the distance of the downstream edge of the exposed electrode to the airfoil trailing edge is zero. (a) Lift coefficient; (b) drag coefficient; (c) lift-to-drag ratio.

The control effect for configuration 2 is presented in Fig. 3. In comparison with configuration 1, the distance of the downstream edge of the right exposed electrode to the airfoil trailing edge is zero. It is shown that the lift

coefficient for the control case is shifted upwards obviously in comparison with the natural case. The maximum lift coefficient at $\alpha$ = 10° is increased by about 5%. On the other hand, the drag coefficient is also increased, and the lift-to-drag ratio is decreased with the plasma control. Such control effect is similar to that induced by the mechanical Gurney flaps. The comparison between configurations 1 and 2 suggests that the right plasma actuator might play a more important role in the lift increment.

Finally, configuration 3 is proposed, where only the right plasma actuator in Fig. 1 is actuated at the same power with configurations 1 and 2. Thus, there will be a horizontal wall jet induced by the plasma actuator with its direction opposite to the free stream. The control effect is shown in Fig. 4. A more significant lift increment than configurations 1 and 2 is obtained. The maximum lift coefficient at $\alpha$ = 10° is increased by about 10%. Although the drag coefficient is also increased with plasma control, the lift-to-drag ratio before stall is increased, with an increase in the maximum lift-to-drag ratio by about 5%. Thus, among the three configurations of the plasma Gurney flap, configuration 3 can best simulate the lift-enhancement characteristics of the mechanical Gurney flap.

### 3.2 Flow Field

In order to reveal the physics of lift increment by the plasma Gurney flap, flow field around the airfoil is measured by PIV. Figure 5(a) shows the time-averaged velocity superposed with velocity vector for the natural case, which shows a small flow separation there. Thus, there is a recirculation region downstream of the airfoil trailing edge, which is extended to about $x/c = 0.12$ and symmetric about the $x$ axis.

With plasma control of configuration 1, the scale of the recirculation region downstream of the airfoil trailing edge is reduced with the downstream edge located near about $x/c = 0.04$. However, it is shown that there is a high speed region just near the plasma actuators, which is formed by the interaction between the plasma induced jet and the free stream. Thus, the flow over the pressure surface of the airfoil is

increased by the plasma control, while the flow over the upper surface nearly has no difference in comparison with the natural case.
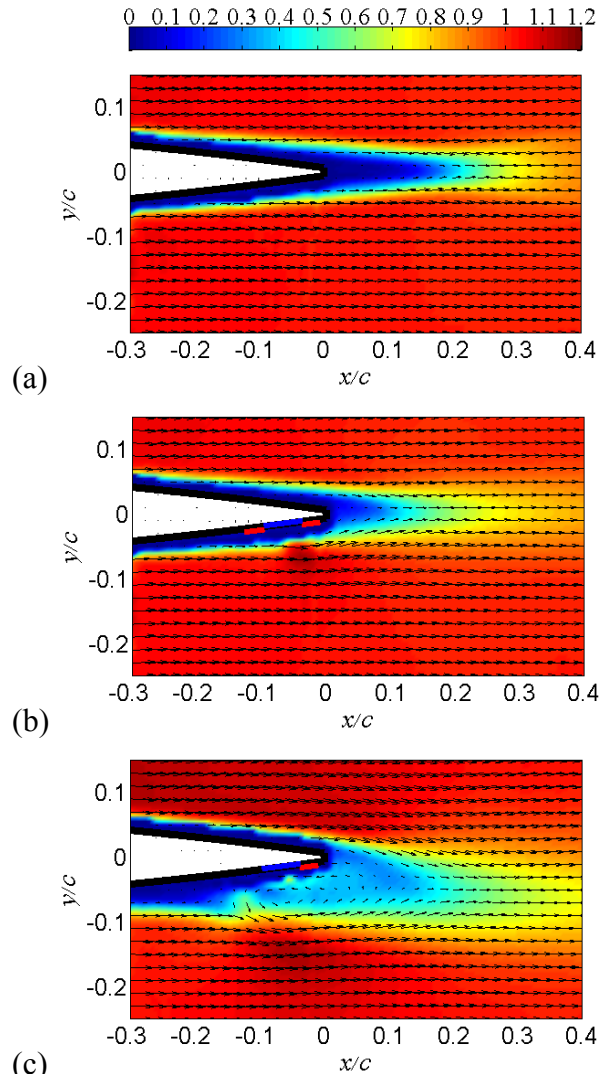


(a)

(b)

(c)

Fig. 5 Time-averaged velocity $\sqrt{U^2+V^2}/U_\infty$ superposed with velocity vector. (a) Natural case; (b) control case with configuration 1: the width of the exposed electrodes and the embedded electrode is 2.5 mm and 6 mm, respectively, and the distance of the downstream edge of the right exposed electrode to the airfoil trailing edge is 1 mm; (c) control case with configuration 3: the width of the exposed electrode and the embedded electrode is 2.5 mm and 6 mm, respectively, and the distance of the downstream edge of the exposed electrode to the airfoil trailing edge is 1 mm.

When the plasma actuator with configuration 3 is applied, the flow over the airfoil shows a large difference compared with the natural case. The interaction between the

plasma induced jet and the free stream results in the formation of a recirculation region just near the plasma actuator over the pressure surface. As a result, the velocity over the pressure surface is decreased, while that over the upper surface is increased. According to the Bernoulli equation, the pressure over the lower surface and the suction over the upper surface should be increased, resulting in an increase in the pressure difference over these surfaces. Thus, the lift coefficient over the airfoil can be improved greatly by this configuration, which is consistent well with the force measurement results shown in Fig. 4. On the other hand, the recirculation region downstream of the airfoil is decreased and the near wake is shifted downwards along the $y$ axis, suggesting that the plasma control increases the equivalent camber of the airfoil. Such variations in the flow topology are similar with those induced by the mechanical Gurney flap. It is also suggested that the proposed plasma Gurney flap in configuration 3 has the similar lift-increment mechanism with the conventional Gurney flap.

## 4 Conclusions

The DBD plasma actuators are used to control the flow around a NACA 0012 airfoil to simulate the lift-increment function of the mechanical Gurney flap, which is named as the plasma Gurney flap. Three different kinds of the plasma Gurney flap have been proposed. For configurations 1 and 2, two DBD plasma actuators are placed onto the pressure surface of the airfoil near the trailing edge to produce a wall-normal jet. The only difference between the two configurations is that the distance of the downstream edge of the second electrode to the airfoil trailing edge. For configuration 3, only one DBD plasma actuator is actuated to produce a horizontal wall jet opposite to the free stream. The force measurement indicates that the configuration 3 can best simulate the mechanical Gurney flap to improve the lift coefficient over the entire angles of attack, while configuration 1 has little influence on the aerodynamic forces. The PIV measurement reveals the control mechanism for the proposed plasma Gurney flap. It is found that the flow topology around the airfoil induced by the plasma Gurney flap of configuration 3 is similar with that induced by the mechanical Gurney flap, suggesting their similar lift-increment mechanism.

## References

[1] Wang JJ, Li YC and Choi K-S. Gurney flap-lift enhancement, mechanisms and applications. *Prog Aerosp Sci*, Vol. 44, pp 22-47, 2008.

[2] Li YC, Wang JJ and Zhang PF. Effect of Gurney flaps on a NACA0012 airfoil. *Flow, Turbulence Combust*, Vol. 68, pp 27-39, 2002.

[3] Li YC, Wang JJ and Zhang PF. Influences of mounting angles and locations on the effects of Gurney flaps. *J Aircraft*, Vol. 40, pp 494-498, 2003.

[4] Liu TS and Montefort J. Thin-airfoil theoretical interpretation for Gurney flap lift enhancement. *J Aircraft*, Vol. 44, pp 667-671, 2007.

[5] Singh MK, Dhanalakshmi K and Chakrabartty SK. Navier-Stokes analysis of airfoils with Gurney flap. *J Aircraft*, Vol. 44, pp 1487-1493, 2007.

[6] Traub LW, Miller A and Rediniotis O. Comparisons of a Gurney and jet-flap for hinge-less control. *J Aircraft*, Vol. 41, pp 420-423, 2004.

[7] Traub LW and Agarwal G. Aerodynamic characteristics of a Gurney/jet flap at low Reynolds numbers. *J Aircraft*, Vol. 45, pp 424-429, 2008.

[8] Jukes TN, Choi K-S, Johnson GA and Scott SJ. Characterization of surface plasma-induced wall flows through velocity and temperature measurements. *AIAA J*, Vol. 44, pp 764-771, 2006.

[9] Moreau E. Airflow control by non-thermal plasma actuators. *J Phys D: Appl Phys*, Vol. 40, pp 605-636, 2007.

[10] Corke TC, Enloe CL and Wilkinson SP. Dielectric barrier discharge plasma actuators for flow control. *Annu Rev Fluid Mech*, Vol. 42, pp 505-529, 2010.

[11] Wang JJ, Choi K-S, Feng LH, Jukes TN and Whalley RD. Recent developments in DBD plasma flow control. *Prog Aerosp Sci*, Vol. 62, pp 52-78, 2013.

[12] Zhang PF, Liu AB and Wang JJ. Aerodynamic modification of a NACA 0012 airfoil by trailing-edge plasma Gurney flap. *AIAA J*, Vol. 47, pp 2467-2474, 2009.

[13] Jukes TN and Choi K-S. Flow control around a circular cylinder using pulsed dielectric barrier discharge surface plasma. *Phys Fluids*, Vol. 21, pp 084103, 2009.

## Copyright Statement